Multicavity X-Ray Fabry-Perot Resonance with Ultrahigh Resolution and Contrast

X. R. Huang,[1,*] D. P. Siddons,[2] A. T. Macrander,[1] R. W. Peng,[3,†] and X. S. Wu[3]

[1]*Advanced Photon Source, Argonne National Laboratory, Argonne, Illinois 60439, USA*

[2]*National Synchrotron Light Source, Brookhaven National Laboratory, Upton, New York 11973, USA*

[3]*National Laboratory of Solid State Microstructures and College of Physics, Nanjing University, Nanjing 210093, China*

(Received 19 November 2011; published 31 May 2012)

Realization of x-ray Fabry-Perot (FP) resonance in back-Bragg-reflection crystal cavities has been proposed and explored for many years, but to date no satisfactory performance has been achieved. Here we show that single-cavity crystal resonators intrinsically have limited finesse and efficiency. To break this limit, we demonstrate that monolithic multicavity resonators with equal-width cavities and specific plate thickness ratios can generate ultrahigh-resolution FP resonance with high efficiency, steep peak tails, and ultrahigh contrast simultaneously. The resonance mechanism is similar to that of sequentially cascaded single-cavity resonators. The ultranarrow-bandwidth FP resonance is anticipated to have various applications, including modern ultrahigh-resolution or precision x-ray monochromatization, spectroscopy, coherence purification, coherent diffraction, phase contrast imaging, etc.

DOI: 10.1103/PhysRevLett.108.224801 PACS numbers: 41.50.+h, 07.60.Ly, 07.85.Nc, 42.25.−p

The Fabry-Perot (FP) interferometer [1] is one of the most fundamental and important optical instruments used in numerous fields for accurate measurements or control of the wavelengths of light and for making lasers [2]. It is typically made of two parallel mirrors that successively reflect light back and forth in the cavity to form interference, which can be implemented for all long-wavelength light to soft x rays [3,4]. Unfortunately, this scheme does not work for hard x rays because there exist no specularly reflecting mirrors for hard x rays at large incidence angles. A solution to this problem is to use backward Bragg diffraction (Bragg angle $\theta_B \simeq 90°$) from two parallel crystal plates to produce x-ray FP interference or resonance, as has been proposed and theoretically explored for many years [5–12].

However, implementation of x-ray FP resonance in crystal cavities has later been demonstrated to be very challenging. For example, only in recent years have Liss *et al.* [13] and Shvyd'ko *et al.* [14] observed from time-resolved transmission measurements the storage of x-ray photons in a few tens of back-and-forth reflection cycles in large crystal cavities (cavity widths 50–150 mm), but their results do not show the resonance fringes, mainly because the incident bandwidth is much larger than the free spectral range of the cavities. The first direct and explicit demonstration of hard x-ray FP resonance fringes was carried out by Chang *et al.* [15,16] using small silicon cavities (40–150 μm). Nevertheless, the FP finesse they measured is only about 2.3, and the resonance peaks have low efficiency with significant background. Several factors might attribute to the underperformance, including the crystal imperfections and strains caused by microelectronic fabrication and the beam divergence caused by the dispersive monochromator [17]. As illustrated below, the most adverse factor is that single crystal cavities intrinsically have limited finesse and efficiency. Without breaking this limitation, such devices could hardly be used for practical applications.

Based on rigorous dynamical theory calculations, we present in this Letter the principles of a more advanced design of x-ray FP resonators, which consists of multiple cavities separated by crystal plates with specific thickness ratios. These resonators are illustrated to have extremely high finesse, sharp tails, and ultralow background, which can completely surpass the limit of conventional crystal-based x-ray optics to achieve unprecedented resolution and coherence and may have versatile applications based on modern synchrotron light sources and free-electron lasers (FELs).

Here we model multicavity resonance based on diamond crystals because they have nearly unity Bragg reflectivity with very low absorption [18,19], based on which the FP mechanisms can be singled out without much complication of absorption. But the main mechanisms still apply to silicon or sapphire cavities. We choose to study the FP resonance within the medium-energy range around 8 keV because most undulators produce higher flux in this range than in the higher-energy range, which is especially critical to medium-energy synchrotrons and FELs. In addition, developing ultrahigh-resolution optics for medium-energy photons has been extremely difficult using conventional crystal optics due to the very wide intrinsic bandwidths of low-order Bragg reflections [20].

Figure 1(a) shows the diamond 224 Bragg reflectivity for different crystal thicknesses t, where the photon energy ΔE is relative to the back-reflection Bragg energy (8.5146 keV). The curve with $t = \infty$ is the spectral Darwin curve of a semi-infinite crystal showing that the strong-reflection Darwin range (indicated by the dashed lines) is $67 < \Delta E < 106$ meV. This is the working energy

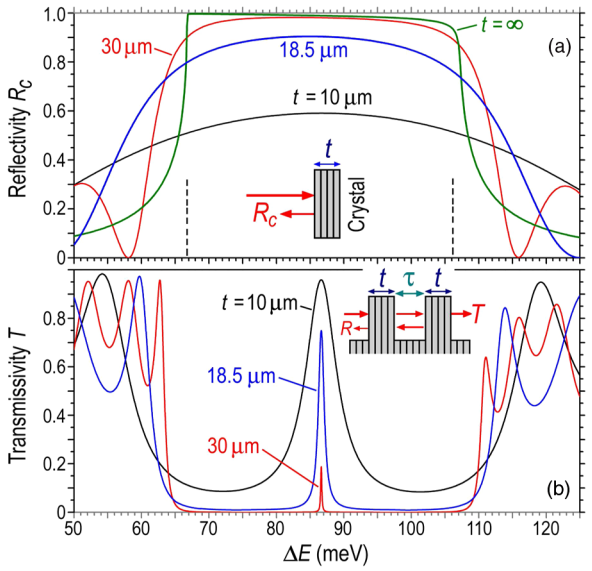

FIG. 1 (color online). (a) Bragg reflectivity of diamond 224 back reflection for different crystal plate thicknesses t. (b) The corresponding transmission spectra of single-cavity resonators. $\tau = 10.9$ μm. The incident angle is 90° −0.5 mrad for avoiding multiple-beam diffraction [15,16,21].

range for FP resonance. The inset in Fig. 1(b) schematically shows a monolithic single-cavity resonator, of which the transmission can be calculated by the rigorous method in the Supplemental Material [21]. The free spectral range of the cavity is $E_f \simeq \frac{1}{2}hc/(\tau + 2\Lambda)$, where τ is the cavity width and Λ is the Bragg-reflection extinction depth (here $\Lambda = 4.88$ μm) (see Supplemental Material [21]). In Fig. 1(b) we set $\tau = 10.9$ μm, corresponding to $E_f = 30$ meV. Under this condition, there is only one resonance peak within the Darwin range (located in the center).

The transmission curves in Fig. 1(b) were calculated with plane-wave incidence and the wave train was assumed to be infinite. As shown in the Supplemental Material [21], a single cavity has maximum resonance efficiency only when the two plates have the same thickness t. So we only consider this situation. When $t = 10$ μm, strong FP resonance occurs in the middle of Fig. 1(b) with peak transmission (efficiency) $T_P = 96\%$. However, the full width at half maximum (FWHM) of the peak is $\delta E = 5.8$ meV, corresponding to low finesse $F = E_f/\delta E = 5.2$. Meanwhile, the background beside the resonance peak is high ($> 8\%$). Obviously, this is due to the low reflectivity, $R_c = 59\%$, of the plates with $t = 10$ μm [Fig. 1(a)].

R_c can be enhanced by increasing t. When $t = 18.5$ μm, R_c reaches 90% in Fig. 1(a), and the corresponding resonance peak width in Fig. 1(b) becomes $\delta E = 1$ meV with $F = 30$. But the peak still has wide tails and the background is still noticeable. Moreover, the finesse improvement is accompanied by the peak efficiency drop to $T_P = 75\%$. [For crystals (e.g., silicon) with higher absorption, the efficiency drops more dramatically with increasing t.] For $t = 30$ μm ($R_c = 98\%$), T_P is only 18% although the peak becomes extremely narrow with $\delta E = 0.19$ meV.

Therefore, a single cavity is generally unable to achieve high finesse and efficiency simultaneously, especially for high-absorption crystals (that also have limited R_c) (see Supplemental Material [21]). A possible way to surmount this obstacle is to sequentially cascade two single-cavity resonators, as shown in Fig. 2(a). However, here the backward wave from the second resonator may either form undesirable resonance in the gap between the two resonators or enter the first cavity to interfere with the waves there. So an "isolator" is desirable to absorb this wave [22]. Under this condition, the total transmission is simply $T = T_s^2$, where T_s is the transmissivity of a single resonator. The dashed line in Fig. 2(c) is the calculated transmission curve of two cascaded resonators. Compared with the transmission curve of the single resonator with $t = 10$ μm in Fig. 1(b), here the peak is narrower, $\delta E = 3.75$ meV, and the peak efficiency is still high, $T_P = 92\%$. More importantly, the background is remarkably suppressed although R_c is only 59%.

Since cascading two resonators requires stringent alignment and stability and temperature control, a much simpler scheme is to merge the two middle plates in Fig. 2(a) such that the two resonators become a monolithic two-cavity resonator in Fig. 2(b). The solid line in Fig. 2(c) is the transmission curve of the two-cavity resonator with $t_1 = t_3 = 10$ μm and $t_2 = 20$ μm (doubled), which indeed has the same T_P and δE as the dashed curve. The difference is

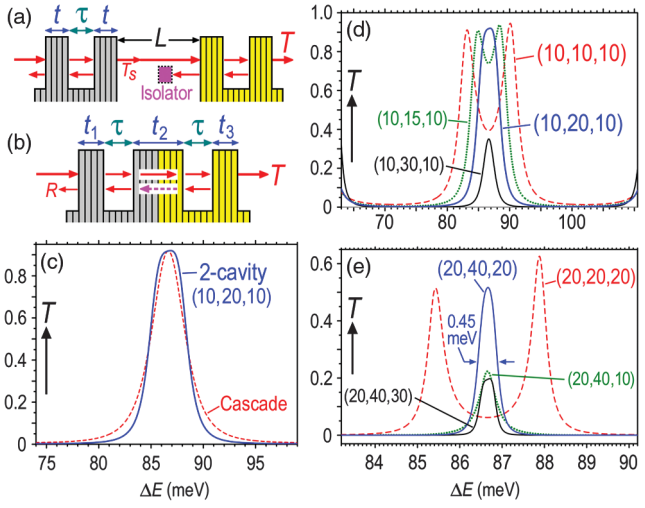

FIG. 2 (color). (a) Cascaded single-cavity resonators. (b) Monolithic two-cavity resonator. (c) Comparison of FP resonance peaks from the cascade of two isolated single-cavity resonators (both with $t = 10$ μm) and a two-cavity resonator with $(t_1, t_2, t_3) = (10, 20, 10)$ μm. (d) and (e) Transmission of two-cavity resonators. All the cavities in (c)–(e) have $\tau = 10.9$ μm with diamond 224 reflection.

that the two-cavity resonance peak has a "fatter body" (corresponding to higher throughput) and steeper tails, which are actually two of the most desirable merits for resonator performance.

In fact, silicon multicavity structures have already been tested by Chang *et al.* [16], but the performance seems much worse than that of single-cavity resonators. The reason is that Chang *et al.* made all the crystal plates equally thick (i.e., periodic structures). We show that this does not work because in Fig. 2(d), the resonance peak of a two-cavity resonator with equal-thickness plates splits into two peaks. Generally for an N-cavity resonator ($N > 1$) with equal-thickness plates, the resonance peak splits into N subpeaks [see Fig. 3(b)]. Thus, for a multicavity resonator to work correctly, the plate thicknesses must be chosen correctly. Figure 2(d) is for optimizing t_2 of the two-cavity resonators with fixed $t_1 = t_3 = 10$ μm. When $t_2 < 2t_1$, the peak always splits, but the two subpeaks tend to merge together when $t_2 \rightarrow 2t_1$, as indicated by the dashed and dotted curves. At $t_2 = 2t_1$, the subpeaks become a single peak. When t_2 increases further, the peak does not split again. Instead, the peak width decreases, but the peak efficiency also decreases (see the curve with $t_2 =$ 30 μm). So $t_1 = t_3 = \frac{1}{2}t_2$ is the optimal condition (which is always true for any Bragg reflections). For example, in Fig. 2(e) when $t_1 = t_3 = 20$ μm [twice that in Fig. 2(d)], the optimal value of t_2 is also doubled to 40 μm. Note that here the peak efficiency is 52% while the peak width is only 0.45 meV ($F = 67$). Combinations of (t_1, t_2, t_3) that do not satisfy $t_1 = t_3 = \frac{1}{2}t_2$ either lead to split peaks or lower efficiency, as shown by other curves in Fig. 2(e).

The optimal condition $t_1 = t_3 = \frac{1}{2}t_2$ indicates that the two-cavity resonance mechanism is indeed similar to that of two cascaded single-cavity resonators. In fact, if we ignore the "isolator" in Fig. 2(a), the two resonators can be considered as a three-cavity structure and our calculation shows that its transmission for $L \rightarrow 0$ is the same as that of the two-cavity resonator in Fig. 2(b) with $t_1 = t_3 = \frac{1}{2}t_2 = t$. Therefore, the two-cavity resonator in Fig. 2(b) is exactly equivalent to the cascaded resonators in Fig. 2(a) with $L \rightarrow 0$ but without the isolator.

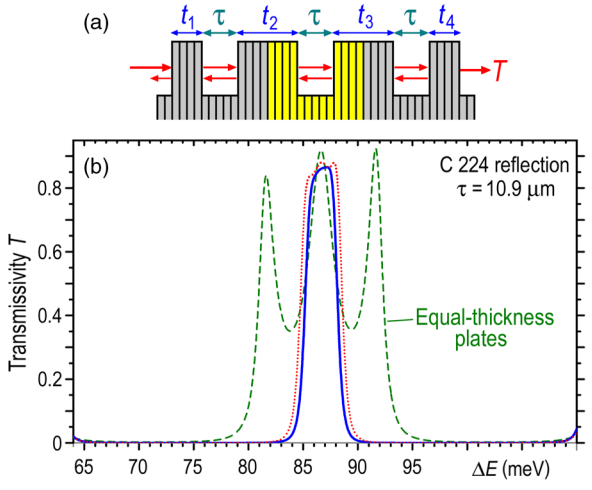

FIG. 3 (color online). (a) Schematic of the three-cavity resonator. (b) Transmission curves of three-cavity resonators. $t_1 = t_4 = 10$ μm. Dashed line: $t_2 = t_3 = 10$ μm. Dotted line: $t_2 = t_3 = 20$ μm. Solid line: $t_2 = t_3 = 22$ μm.

If the isolator exists, it slightly changes the shape of the resonance peak, as can be seen in Fig. 2(c) from the comparison of the dashed curve (calculated with the isolator) with the two-cavity curve [equivalent to that of Fig. 2(a) with $L \rightarrow 0$ and without the isolator]. Nevertheless, the difference is small, indicating that the isolator actually does not play an active role. The reason is that when FP resonance occurs, the backward wave from the second resonator in Fig. 2(a) is minimum, so the isolator has little effect. Out of the resonance range, the *reflectivity* from the second resonator is large. However, here the reflectivity of the first resonator is equally large, which means that the incident beam has already been largely backreflected by the left two plates before reaching the third one. Then, the transmission T_s is small, which makes the reflection from the third plate still very low. Therefore, the backward wave from the second resonator in Fig. 2(a) is always weak with $L \rightarrow 0$ (see Supplemental Material [21]). Equivalently, the backward wave (dashed arrow) in Fig. 2(b) is also always weak for $t_1 = t_3 = t = \frac{1}{2}t_2$ [23]. Thus, the two cavities are largely independent of each other except that the first cavity provides a one-way input to the second cavity; i.e., the resonance processes of the two cavities in Fig. 2(b) occur sequentially with little interaction. Consequently, the x-ray coherence length required for FP resonance only needs to be sufficiently larger than the (small) width τ of a single cavity instead of the length of the entire multicavity resonator.

These mechanisms also apply to N-cavity resonators ($N > 2$). For example, in Fig. 3 when the three-cavity resonator consists of equal-thickness plates, the resonance peak splits into three subpeaks. The subpeaks merge together when t_2 and t_3 are doubled. So the three-cavity resonator is (nearly) equivalent to three cascaded single-cavity resonators. Here the resonator with $t_2 = t_3 = 2t_1 = 2t_4$ has slight bumps on the resonance peak, which, however, can be removed by slightly increasing t_2 and t_3 above $2t_1$, as shown by the curve with $t_2 = t_3 = 22$ μm in Fig. 3(b).

For comparison, Figure 4(a) shows the FP resonance peaks with 1 meV bandwidths generated by optimized single-, two-, and three-cavity resonators, where the background levels of the two- and three-cavity curves are roughly 2 and 4 orders lower than that of the single-cavity curve, respectively.

The multicavity resonators can be used as compact in-line monochromators with ultrahigh energy resolution. For this purpose, a premonochromator must be used to limit

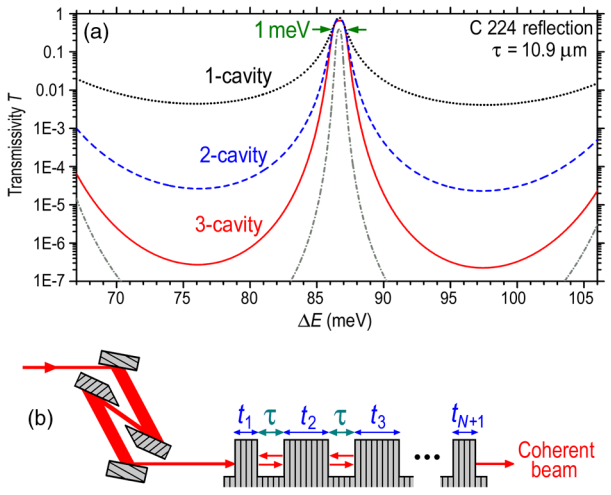

FIG. 4 (color online). Comparison of FP resonance with 1 meV resolution from single-, two-, and three-cavity resonators. Dotted line: $t = 18.5\ \mu$m. Dashed line: $t_1 = \frac{1}{2}t_2 = t_3 = 16.5\ \mu$m. Solid line: $t_1 = t_4 = 14\ \mu$m, $t_2 = t_3 = 32\ \mu$m. The peak efficiencies of the single-, two-, and three-cavity resonators are 75%, 72%, and 67%, respectively. [Dash-dotted line: sub-meV three-cavity resonance, $(t_1, t_2, t_3, t_4) = (18, 40, 40, 18)\ \mu$m, $\delta E = 0.4$ meV, and $T_P = 40\%$.] (b) Combining the N-cavity resonator with the nested channel-cut premonochromator to produce a highly monochromatic and coherent beam.

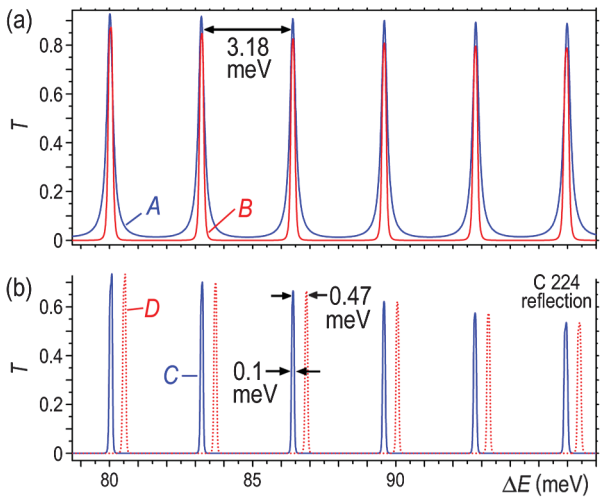

FIG. 5 (color). FP resonance of large cavities. $\tau = 185.3\ \mu$m. (a) Curve A: single-cavity resonance with $t_1 = t_2 = 14\ \mu$m. Curve B: two-cavity resonance with $t_1 = \frac{1}{2}t_2 = t_3 = 14\ \mu$m. (b) Curve C: three-cavity resonance with $t_1 = t_4 = 14\ \mu$m and $t_2 = t_3 = 32\ \mu$m. Curve D was calculated with the incidence direction changed from that of curve C by 100 μ rad. See the log scales in the Supplemental Material [21].

the incidence bandwidth within the Darwin range. As shown in Fig. 4(b), here one can use a silicon nested channel-cut premonochromator [17,24,25] to produce a bandwidth <20 meV (compared with the Darwin width of 39 meV here). Following it the multicavity resonator can further monochromatize the beam to meV or sub-meV bandwidths. Afterwards, the highly monochromatic beam can be used for ultrahigh-resolution diffraction, spectroscopy, metrology, etc. The monochromatized beam also has ultrahigh coherence, particularly temporal coherence, due to the narrow bandwidth. Hence, it can be used for ultrahigh-resolution coherent diffraction and phase contrast imaging.

The resolution can be further improved to 0.1 meV or even up to μ eV in principle [14,21] by increasing τ. Figure 5 shows the FP resonance spectra of multicavity resonators with $\tau = 185.3\ \mu$m (for all the cavities), corresponding to $E_f = 3.178$ meV. Under this condition, there exist a series of resonance peaks within the Darwin range. The peak widths of the single- and two-cavity resonance in Fig. 5(a) are $\delta E = 0.24$ and 0.16 meV, respectively. The three-cavity resonance peaks in Fig. 5(b) have $\delta E = 0.1$ meV with needlelike shapes (close to Gaussian distribution). Curve D in Fig. 5(b) shows that the resonance peaks shift with the incidence direction by a (linear) rate 4.7 μ eV/μ rad [25].

Note that curves A, B, and C (with different plate thicknesses but with the same τ) have the same peak positions, which are determined only by τ. This indicates that FP resonance occurs only in the cavities and is absent in the plates (i.e., the plates do not act as FP etalons). Thus, the cavity widths should be well controlled to be the same during fabrication. Our calculations show that the error tolerance is less than 0.1 μm for the above typical parameters (which means that the surface roughness should also be less than 0.1 μm). By contrast, the error tolerance of the plate thicknesses is generally 1 μm or more [12]. However, crystal defects and lattice constant variations can significantly affect the FP performance, but nowadays nearly perfect "type IIa" diamond crystals with homogeneous reflectivity close to 100% are commercially available [19,21].

Also note that one may place the resonator with 0.1 meV (or better) resolution after the 1-meV resonator in Fig. 4(b) to produce a 0.1-meV-bandwith beam from a white beam [11,26]. Fascinatingly, the two resonators can again be merged into a monolithic structure with two different cavity widths (see Supplemental Material [21] for details). This could lead to significant breakthroughs since developing unprecedented sub-meV-resolution optics at medium energies has been aggressively pursued but with daunting challenges in recent years for modern medium-energy synchrotron light sources [20,27].

In summary, we have demonstrated that simple multicavity resonators with equal-width cavities and with specific plate thickness ratios can produce ultrahigh-resolution FP resonance (up to μ eV) with high efficiency, steep tails, and ultralow background simultaneously. Based on the fact that the resonance mechanisms are similar to those

of cascaded resonators, more complicated monolithic cavity arrays, even with varying cavity widths, can also be designed and implemented (see Supplemental Material [21]). The unprecedented resolving power of multicavity x-ray resonance may have a variety of novel applications, and the underlying mechanisms may also shed light on many other resonance phenomena.

X. R. H. thanks L. Young, C. Jacobsen, and L. Assoufid for helpful discussions and support. This work was supported by the U.S. Department of Energy, Office of Science, Office of Basic Energy Sciences, under Contracts No. DE-AC02-06CH11357 and DEAC-02-98CH10886. R. W. P. was supported by the MOST of China (Grants No. 2012CB921502 and 2010CB630705), the NSFC (Grants No. 11034005, 61077023, and 11021403), and partly by Jiangsu Province Grant No. BK2008012. X. S. W. was supported by the National Key Projects for Basic Researches of China (Grant No. 2010CB923404) and the NSFC (Grants No. 10974081 and 10971079).

*xiahuang@aps.anl.gov
†rwpeng@nju.edu.cn

[1] C. Fabry and A. Pérot, Ann. Chim. Phys. **7**, 115 (1899).
[2] J. M. Vaughan, *The Fabry-Perot Interferometer: History, Theory, Practice and Applications* (Taylor & Francis, New York, 1989).
[3] W. L. Bond, M. A. Duguay, and P. M. Rentzepis, Appl. Phys. Lett. **10**, 216 (1967).
[4] N. M. Ceglio, D. P. Gaines, J. E. Trebes, R. A. London, and D. G. Stearns, Appl. Opt. **27**, 5022 (1988).
[5] R. D. Deslattes, Appl. Phys. Lett. **12**, 133 (1968).
[6] M. Hart, Rep. Prog. Phys. **34**, 435 (1971).
[7] A. Steyerl and K.-A. Steinhauser, Z. Phys. B **34**, 221 (1979).
[8] A. Caticha and S. Caticha-Ellis, Phys. Rev. B **25**, 971 (1982).
[9] R. Colella and A. Luccio, Opt. Commun. **50**, 41 (1984).
[10] A. Caticha and S. Caticha-Ellis, Phys. Status Solidi A **119**, 643 (1990).
[11] S. Kikuta, Y. Imal, T. Iizuka, Y. Yoda, X.-W. Zhang, and K. Hirano, J. Synchrotron Radiat. **5**, 670 (1998).
[12] V. G. Kohn, Yu. V. Shvyd'ko, and E. Gerdau, Phys. Status Solidi B **221**, 597 (2000).
[13] K.-D. Liss, R. Hock, M. Gomm, B. Waibel, A. Magerl, M. Krisch, and R. Tucoulou, Nature (London) **404**, 371 (2000).
[14] Yu. V. Shvyd'ko, M. Lerche, H.-C. Wille, E. Gerdau, M. Lucht, H. D. Rüter, E. E. Alp, and R. Khachatryan, Phys. Rev. Lett. **90**, 013904 (2003).
[15] S.-L. Chang, Yu. P. Stetsko, M.-T. Tang, Y.-R. Lee, W.-H. Sun, M. Yabashi, and T. Ishikawa, Phys. Rev. Lett. **94**, 174801 (2005).
[16] S.-L. Chang *et al.*, Phys. Rev. B **74**, 134111 (2006).
[17] X. R. Huang, A. T. Macrander, M. G. Honnicke, Y. Q. Cai, and P. Fernandez, J. Appl. Crystallogr. **45**, 255 (2012).
[18] Yu. V. Shvyd'ko, S. Stoupin, A. Cunsolo, A. H. Said, and X. Huang, Nature Phys. **6**, 196 (2010).
[19] Yu. Shvyd'ko, S. Stoupin, V. Blank, and S. Terentyev, Nature Photon. **5**, 539 (2011).
[20] See http://www.bnl.gov/nsls2/design.asp and http://www.bnl.gov/ps/nsls2/beamlines/files/pdf/IXS_pdr.pdf for the background and importance of ultrahigh-resolution medium-energy x-ray optics.
[21] See Supplemental Material at http://link.aps.org/supplemental/10.1103/PhysRevLett.108.224801 for dynamical theory calculations of multicavity crystals and for more properties of multicavity resonance.
[22] The isolator is possible only when the backward and forward waves are spatially separated. Otherwise an alternative way may be to make the distance between the two resonators much larger than the x-ray coherence length. A. A. M. Saleh and J. Stone, J. Lightwave Technol. **7**, 323 (1989).
[23] On the two-cavity resonance peak in Fig. 2(c) ($T_P = 92\%$), the crystal absorption is only 8% (with negligible reflection R), close to the single-pass linear absorption of the three plates (4.5%), indicating that multiple back-and-forth x-ray transmission through the plates (particularly the middle plate) is indeed largely absent during the resonance (but multiple reflections always occur in the cavities).
[24] T. Ishikawa, Y. Yoda, K. Izumi, C. K. Suzuki, X. W. Zhang, M. Ando, and S. Kikuta, Rev. Sci. Instrum. **63**, 1015 (1992).
[25] Note that in Refs. [15,16] the premonochromator used was a *dispersive* four-bounce monochromator. M. Yabashi, K. Tamasaku, S. Kikuta, and T. Ishikawa, Rev. Sci. Instrum. **72**, 4080 (2001); M. Yabashi, K. Tamasaku, and T. Ishikawa, Phys. Rev. Lett. **87**, 140801 (2001). A dispersive four-bounce monochromator is detrimental for sub-meV resonance since it always produces a divergent beam even if the incident beam is a strictly parallel beam, while the nondispersive nested channel cuts in Fig. 4(b) exactly preserve the incident wave directions [17].
[26] W. V. Houston, Phys. Rev. **29**, 478 (1927).
[27] Y. Shvyd'ko, S. Stoupin, D. Shu, and R. Khachatryan, Phys. Rev. A **84**, 053823 (2011); X.-R. Huang, J. Synchrotron Radiat. **18**, 899 (2011).